

**DEVELOPMENT OF NANOCASTED TIN OXIDE
FOR ETHANOL AND ACETONE GAS SENSOR**

JUSLIHA BINTI JUHARI

UNIVERSITI SAINS MALAYSIA

2018

**DEVELOPMENT OF NANOCASTED TIN OXIDE FOR ETHANOL AND
ACETONE GAS SENSOR**

by

JUSLIHA BINTI JUHARI

**Thesis Submitted in Fulfilment of the
Requirements for the Degree of
Doctor of Philosophy**

September 2018

ACKNOWLEDGEMENT

Alhamdulillah praises to the Almighty God, Allah S.W.T upon the strengths and His blessing in completing this thesis. A special appreciation goes to my supervisor, Associate Professor Dr. Mohamad Zailani Abu Bakar, for his breaking through ideas and valuable guidance throughout the research work, which are essential to make this thesis possible. Great thanks to my co-supervisor, Professor Dr. Ahmad Zuhairi Abdullah, for his incessant support, encouragement and knowledge regarding this research topic.

I would like to express my gratitude to the Dean School of Chemical Engineering (SCE), Professor Dr. Azlina Harun @ Kamaruddin for the administration support and help towards my postgraduate affairs. My special thanks to all SCE academic, administration and technical staff for their kindness and cooperation. I would like to extend my heartiest appreciation to Ministry of Higher Education (MOHE) for providing me with MyPhD scholarship to assist my studies financially and the allocation for funding this research work through FRGS grant (6071250). Thanks also to Universiti Sains Malaysia (USM) for providing RU-PRGS grant (8046002) and RUI grant (814221) for this research work.

I am indeed very thankful to my lovely husband, Mr. Mohd Hilmi Abdullah, my adorable princes; Muaz Hakimi Mohd Hilmi and Muhammad Anas Mohd Hilmi, my adored parents; Mr. Juhari Saad and Mrs. Siti Zaliha Abdullah, as well as my beloved sisters and brothers. They are always on my side, riding along with my difficulties. Finally, to my dear friends, thanks for your kind supports and soothing words.

Jusliha Juhari, September 2018

TABLE OF CONTENTS

	Page
ACKNOWLEDGEMENT	ii
TABLE OF CONTENTS	iii
LIST OF TABLES	viii
LIST OF FIGURES	x
LIST OF ABBREVIATIONS	xvii
LIST OF SYMBOLS	xxi
ABSTRAK	xxii
ABSTRACT	xxiv
CHAPTER ONE: INTRODUCTION	
1.1 Importance of Air Pollutant Monitoring	1
1.2 Detection and Monitoring System	5
1.2.1 Conventional Analytical Instrument	6
1.2.2 Solid-State Gas Sensors	7
1.3 Metal Oxide-based Semiconductor Gas Sensors	9
1.4 Mesoporous Metal Oxides	16
1.5 Problem Statement	17
1.6 Research Objectives	21
1.7 Scope of the Study	21
1.8 Organization of the Thesis	23
CHAPTER TWO: LITERATURE REVIEW	
2.1 Overview of Porous Materials	26
2.1.1 Classification of Porous Materials	26
2.1.2 Ordered Mesoporous Silica	29

2.2	Ordered Mesoporous Metal Oxides	33
2.3	Synthesis Methods for Ordered Mesoporous Metal Oxides	36
2.3.1	Soft-templating Method	37
2.3.2	Hard-templating Method (Nanocasting)	41
2.3.2(a)	The Concept of Nanocasting	42
2.3.2(b)	Ordered Mesoporous Silica as Hard Template	45
2.3.3	Nanocasting Parameters of Ordered Mesoporous Metal Oxides	55
2.3.3(a)	Selection of Silica Template	55
2.3.3(b)	Selection of Precursors and Solvent	61
2.3.3(c)	Infiltration of Metal Precursor into the Pore of Silica Template	63
2.3.3(d)	Conversion of Metal Precursor	66
2.3.3(e)	Methods for Removing Silica Template	67
2.4	Application of Ordered Mesoporous Metal Oxides in Gas Sensing	68
2.5	Gas-Sensing Mechanism	75
2.6	Ordered Mesoporous SnO ₂ as a Sensor Material	80
2.7	Concluding Remarks	83
 CHAPTER THREE: MATERIALS AND METHODS		
3.1	Chapter Overview	85
3.2	Materials, Chemicals and Gases	85
3.3	Equipment	88
3.4	Preparation of Ordered Mesoporous Sensing Materials	89
3.4.1	Synthesis of Hard Templates	89
3.4.1(a)	Ordered Mesoporous Silica KIT-6	89
3.4.1(b)	Ordered Mesoporous Silica SBA-15	90
3.4.1(c)	Ordered Mesoporous Silica SBA-16	90

3.4.2	Nanocasting of Ordered Mesoporous SnO ₂ Materials	91
3.4.2(a)	Effect of Type of Ordered Mesoporous Silica (OMS)	91
3.4.2(b)	Effect of Hydrothermal Aging Temperature of OMS	93
3.4.2(c)	Effect of Infiltration Method	93
3.4.2(d)	Effect of Cycle of Infiltration Step	95
3.4.2(e)	Effect of Additive Loading Technique	96
3.4.2(f)	Effect of Additive Loading	97
3.4.3	Thermal Stability of Ordered Mesoporous Sensing Materials	99
3.5	Fabrication of Thick Film Gas Sensors	100
3.6	Characterization of Ordered Mesoporous Sensing Materials	101
3.6.1	Powder X-ray Diffraction (P-XRD) Analysis	102
3.6.2	Surface Area (Nitrogen Adsorption-Desorption) Analysis	102
3.6.3	Transmission Electron Microscopy (TEM) Analysis	103
3.6.4	Scanning Electron Microscopy (SEM) and Energy Dispersive X-ray (EDX) Analysis	103
3.6.5	Thermogravimetric (TG) and Differential Scanning Calorimetry (DCS) Analysis	105
3.6.6	UV-vis Diffuse Reflectance Spectroscopy (UV-vis DRS) Analysis	105
3.7	Measurement of Gas-Sensing Performance	105
3.7.1	Description of Experimental Set-Up	105
3.7.1(a)	Calibration of Detected Gas Concentration	107
3.7.1(b)	Circuiting of the Measurement Unit	108
3.7.1(c)	Data Logging	110
3.7.2	Experimental Procedures	112
3.7.2(a)	Electrical Resistivity and Sensitivity Measurement	112
3.7.2(b)	Response and Recovery Time	114
3.7.3	Operating Parameter Studies	115

3.7.3(a)	Optimum Operating Temperature	116
3.7.3(b)	Selectivity towards Different Target Gases	116
3.7.3(c)	Variation of Gas Concentrations	117
3.7.3(d)	Response and Recovery Times	117
3.7.3(e)	Stability of the Gas Sensor	117

CHAPTER FOUR: RESULTS AND DISCUSSION

4.1	Chapter Overview	118
4.2	Characterization of Ordered Mesoporous Silica as a Hard Template	118
4.2.1	KIT-6 Silica Template	119
4.2.2	SBA-15 Silica Template	129
4.2.3	SBA-16 Silica Template	133
4.2.4	Summary	138
4.3	Nanocasting of Ordered Mesoporous SnO ₂ using Different Silica Templates	139
4.3.1	Effects of Type of Ordered Mesoporous Silica	140
4.3.1(a)	Structural and Textural Properties	140
4.3.1(b)	Sensitivity towards Ethanol Vapour	152
4.3.2	Effects of Hydrothermal Aging Temperature of Silica Template	155
4.3.2(a)	Structural and Textural Properties	155
4.3.2(b)	Sensitivity towards Ethanol Vapour	162
4.3.3	Summary	162
4.4	Nanocasting of Highly Ordered Mesoporous SnO ₂ with Different Infiltration Methods	163
4.4.1	Conversion of SnO ₂ precursor in KIT-6 silica template	164
4.4.2	Effects of Infiltration Method	167
4.4.2(a)	Structural and Textural Properties	167

4.4.2(b)	Sensitivity towards Ethanol Vapour	172
4.4.3	Summary	173
4.5	Nanocasting of Highly Ordered Mesoporous SnO ₂ Loaded with Acid and Basic Oxides	174
4.5.1	Effects of Additive Loading	174
4.5.1(a)	Structural and Textural Properties	174
4.6	Performance of the Optimum Sensors under Various Operating Parameters	182
4.6.1	Optimum Operating Temperature	183
4.6.2	Selectivity towards Different Target Vapours	187
4.6.3	Variation of Ethanol Concentrations	190
4.6.4	Response and Recovery Times	194
4.6.5	Stability of the Sensor	196
4.7	Ethanol-Sensing Mechanism of Sensor based on Ordered Mesoporous 5.0LS(K80)-V(2)-DS	198

CHAPTER FIVE: CONCLUSIONS AND RECOMMENDATIONS

5.1	Conclusions	201
5.2	Recommendations	203

REFERENCES	205
-------------------	-----

APPENDICES

Appendix A: Photo of the Experiment Rig Set-up

Appendix B: Calibration Curve

Appendix C: Gas Chromatography Analysis

LIST OF PUBLICATIONS

LIST OF TABLES

		Page
Table 1.1	Solid-state gas sensors for detecting environmental gases (Hu et al., 2010).	10
Table 1.2	Sign of resistance change (increase or decrease) to change in gas atmosphere (Williams, 1999).	13
Table 1.3	Classification of metal oxides based on type of conductivity (Korotcenkov, 2007).	13
Table 1.4	Band gap of metal oxide used as sensing materials (Korotcenkov, 2007).	14
Table 2.1	Overview of OMMOs synthesized by soft-templating methods.	39
Table 2.2	Summary of OMMOs synthesized by nanocasting method using OMS as the hard templates.	47
Table 2.3	Summary of the reported OMMOs prepared via nanocasting method with different synthesis parameters.	69
Table 2.4	Summary of the OMMOs synthesized via nanocasting method using OMS as hard templates for gas sensor applications.	76
Table 3.1	List of materials, chemicals and gases required in the research activities.	87
Table 3.2	List of equipment required in the research activities.	88
Table 3.3	Synthesis parameters studied in the nanocasting of ordered mesoporous SnO ₂ materials.	99
Table 3.4	Summary on analytical techniques used for the characterization of ordered mesoporous sensing materials.	101
Table 3.5	Retention time of standard reference, standard gas and sample of detected gas.	108

Table 4.1	Textural properties of 3-D cubic mesoporous KIT-6 silica templates with different hydrothermal aging temperatures.	124
Table 4.2	Textural properties of 2-D hexagonal mesoporous SBA-15 silica template synthesized at a hydrothermal aging temperature of 80 °C.	132
Table 4.3	Textural properties of 3D cubic with cage-like pore mesoporous SBA-16 silica template synthesized at a hydrothermal aging temperature of 28 °C.	137
Table 4.4	Crystallite size of mesoporous SnO ₂ materials replicated from different OMS templates.	144
Table 4.5	Textural properties of mesoporous SnO ₂ materials replicated from different OMS templates.	149
Table 4.6	Crystallite size of mesoporous SnO ₂ materials replicated from KIT-6 silica template of different hydrothermal aging temperatures.	158
Table 4.7	Textural properties of mesoporous SnO ₂ materials replicated from KIT-6 silica template of different hydrothermal aging temperatures.	161
Table 4.8	Crystallite size of ordered mesoporous SnO ₂ replicas with different infiltration methods.	169
Table 4.9	Textural properties of ordered mesoporous SnO ₂ replicas with different infiltration methods.	169
Table 4.10	Textural properties of the ordered mesoporous SnO ₂ synthesized at different additives loadings.	181
Table 4.11	Selectivity value for S(K80)-VASEM(2), 5.0LS(K80)-V(2)-DS and 10.0LS(K80)-V(2)-DS sensors at various concentrations of vapours.	190
Table 4.12	Response time and recovery time for the S(K80)-VASEM(2) and 5.0LS(K80)-V(2)-DS sensors.	196

LIST OF FIGURES

		Page
Figure 1.1	Concentration levels of typical gas components concerned in Japan (Yamazoe, 2005).	2
Figure 1.2	Toxic gases effects on human health (Leghrib, 2010)	4
Figure 1.3	(a) the changes in the gas concentration of metal oxide-based semiconductor gas sensor with n-type conductivity; (b) the gas is applied at t_1 , t_3 and removed at t_2 , t_4 ; (c) lead to changes in the conductance G or resistance R of the sensor (Gurlo and Riedel, 2007).	12
Figure 1.4	Relative comparison of different metal oxides used for gas-sensing application (Eranna et al., 2004).	15
Figure 2.1	Classification of porous materials into microporous, mesoporous, and macroporous materials according to their pore size diameters and typical pore size distributions (Ariga et al., 2012).	27
Figure 2.2	Mesotstructures of M41S family: (a) mesoporous 2-D hexagonal MCM-41 silica, (b and c) mesoporous 3-D cubic MCM-48 silica and (d) lamellar MCM-50 silica (Selvam et al., 2001).	30
Figure 2.3	Schematic pathway for preparing surfactant-templated OMS, illustrating a formation mechanism based on a pre-formed liquid-crystal (LC) mesophase (route A) or a cooperative self-assembly process (route B) (Walcarius, 2013).	32
Figure 2.4	TEM images of 2-D hexagonal mesoporous TiO ₂ (a), ZrO ₂ (b), Nb ₂ O ₅ (c), SnO ₂ (d), WO ₃ (e), Al ₂ O ₃ (f), SiTiO ₄ (g), and SiAlO _{3.5} (h) (Yang et al. 1998).	35
Figure 2.5	Schematic illustration of the hard-templating (nanocasting) pathway leading to ordered mesoporous metal oxides (Lu et al., 2010).	43

Figure 2.6	(a) Mesostucture model, (b) TEM image for cross section of the hexagonally ordered Cr ₂ O ₃ nanorods and (c) HRTEM image of 3-D mesoporous Cr ₂ O ₃ (the arrows indicate the small bridges between the rods) (Zhu et al., 2003).	46
Figure 2.7	TEM images and SAED patterns of OMMOs templated by MWD-SBA-15 and MWD-SBA-16 silica (A) Cr ₂ O ₃ nanowires, (B) Mn _x O _y , (C) Fe ₂ O ₃ nanowires, (D) Co ₃ O ₄ nanowires, (E) NiO nanowires, (F) In ₂ O ₃ nanowires, (G) CeO ₂ nanowires and (H) Co ₃ O ₄ nanospheres (Tian et al., 2003c).	52
Figure 2.8	TEM images of ordered mesoporous CeO ₂ synthesized with (a) 3-D cubic <i>Ia3d</i> silica template, and b) 2-D hexagonal <i>p6mm</i> silica template (Laha and Ryoo, 2003).	53
Figure 2.9	Photograph (top) and SEM images (bottom) of a hierarchically porous SiO ₂ monolith and the respective Co ₃ O ₄ , SnO ₂ , and Mn ₂ O ₃ monolith replicas (Smatt et al., 2006).	54
Figure 2.10	Schematic illustration of formation of (A) disordered structure using MCM-41 with disconnected pores system and (B) ordered structures using SBA-15 with an interconnected pore system (Ryoo et al., 2001).	56
Figure 2.11	Schematic illustration of formation of (a) <i>p6mm</i> ordered structure using SBA-15, (b) <i>Im3m</i> ordered structures using SBA-16 and (c) <i>Ia3d</i> ordered structures with KIT-6 (Kumar and Chowdhury, 2015).	59
Figure 2.12	The effects of hydrothermal aging temperature on the pore structure of SBA-15 silica at (a) low temperature (35-60 °C), (b) moderate temperature (80-100 °C) and (c) high temperature (>120 °C) (Galarneau et al., 2003).	60
Figure 2.13	(a) Dynamic response and (b) response time of pure WO ₃ replicas of SBA-15 and KIT-6 to different concentrations of NO ₂ in synthetic air at operating temperature of 230 °C (Rossinyol et al., 2007a).	73

Figure 2.14	Correlation between the sensitivity and structural properties of the In ₂ O ₃ samples: (a) sensitivity vs. specific BET surface area; (b) surface-normalized sensitivity vs. average pore width; (c) surface-normalized sensitivity vs. average pore wall thickness (Waitz et al., 2009).	74
Figure 2.15	Gas-sensing mechanism of n-type metal oxide semiconductors E_c , E_f and E_v denote the energy of the conduction band, Fermi level and valence band, respectively, while eV_{surface} denotes the potential barrier. The conducting electrons are represented by e^- (Zhou et al., 2017).	75
Figure 3.1	Flowchart of experimental works involved in the research activities.	86
Figure 3.2	Flowchart of parameters studied in the nanocasting of ordered mesoporous SnO ₂ materials.	92
Figure 3.3	Synthesis parameter for nanocasting of ordered mesoporous SnO ₂ with different types of OMS.	94
Figure 3.4	Synthesis procedure for nanocasting of ordered mesoporous SnO ₂ through vacuum-assisted solvent evaporation method (VASEM).	96
Figure 3.5	Synthesis procedure for nanocasting of ordered mesoporous SnO ₂ loaded with WO ₃ and La ₂ O ₃ through direct synthesis (DS) of loading technique.	98
Figure 3.6	Schematic drawing of the SnO ₂ thick film gas sensor.	100
Figure 3.7	Schematic diagram of sensor measurement unit.	106
Figure 3.8	Schematic series for R-V electronic circuit.	109
Figure 3.9	Sketch of I-V graph.	110
Figure 3.10	Generalized response graph of the thick-film sensor during the electrical resistivity and sensitivity measurement.	113
Figure 3.11	The response time of the thick-film sensor.	115
Figure 3.12	The recovery time of the thick-film sensor.	115

Figure 4.1	Small-angle XRD patterns of mesoporous KIT-6 silica templates synthesized at different hydrothermal aging temperatures; (a) KIT-6-60, (b) KIT-6-80 and (c) KIT-6-100.	120
Figure 4.2	N ₂ adsorption–desorption isotherms (A) and the corresponding pore size distributions (B) of mesoporous KIT-6 silica templates synthesized at different hydrothermal aging temperatures; (a) KIT-6-60, (b) KIT-6-80 and (c) KIT-6-100.	122
Figure 4.3	SEM images of mesoporous KIT-6 silica templates synthesized at different hydrothermal aging temperatures; (a, b) KIT-6-60, (c, d) KIT-6-80 and (e, f) KIT-6-100. Magnification: 5000x (a, c, e) and 10000x (b, d, f).	126
Figure 4.4	TEM images for the cross-sectional and perpendicular views of mesoporous KIT-6 silica templates synthesized at different hydrothermal aging temperatures; (a-b) KIT-6-60, (c-d) KIT-6-80 and (e-f) KIT-6-100. Magnification: 35000x.	128
Figure 4.5	Small-angle XRD pattern of mesoporous SBA-15 silica template synthesized at a hydrothermal aging temperature of 80 °C.	129
Figure 4.6	N ₂ adsorption-desorption isotherm (A) and their corresponding pore size distribution (B) of mesoporous SBA-15 silica template synthesized at a hydrothermal aging temperature of 80 °C.	130
Figure 4.7	SEM (a, b) and TEM (c, d) images of mesoporous SBA-15 silica template synthesized at a hydrothermal aging temperature of 80 °C. Magnification for SEM: 10000x (a) and 20000x (b), Magnification for TEM: 45000x (c, d).	133
Figure 4.8	Small-angle XRD pattern of mesoporous SBA-16 silica template synthesized at a hydrothermal aging temperature of 28 °C.	134
Figure 4.9	N ₂ adsorption-desorption isotherm (A) and their corresponding pore size distribution (B) of mesoporous SBA-16 silica template synthesized at a hydrothermal aging temperature of 28 °C.	135

Figure 4.10	SEM (a, b) and TEM (c, d) images of mesoporous SBA-16 silica template synthesized at a hydrothermal aging temperature of 28 °C. Magnification for SEM: 10000x (a) and 20000x (b). Magnification for TEM: 45000x.	138
Figure 4.11	Small-angle XRD patterns of mesoporous SnO ₂ materials replicated from different OMS templates; (a) SnO ₂ (K6-60), (b) SnO ₂ (S15-80), and (c) SnO ₂ (S16-28).	141
Figure 4.12	Wide-angle XRD patterns of (A) SnO ₂ commercial and (B) mesoporous SnO ₂ materials replicated from different OMS templates; (a) SnO ₂ (K6-60), (b) SnO ₂ (S15-80), and (c) SnO ₂ (S16-28).	143
Figure 4.13	N ₂ adsorption-desorption isotherms and respective pore size distributions (insets) of (a) SnO ₂ commercial and mesoporous SnO ₂ materials replicated from different OMS templates; (b) SnO ₂ (K6-60), (c) SnO ₂ (S15-80) and (d) SnO ₂ (S16-28).	146
Figure 4.14	TEM images of (a) SnO ₂ commercial and mesoporous SnO ₂ replicated from different OMS templates; (b) SnO ₂ (K6-60), (c) SnO ₂ (S15-80) and (d) SnO ₂ (S16-28). Magnification: 35000x.	150
Figure 4.15	SEM images of (a) SnO ₂ commercial and mesoporous SnO ₂ materials replicated from different OMS templates; (b) SnO ₂ (K6-60), (c) SnO ₂ (S15-80) and (d) SnO ₂ (S16-28). Magnification: 5000x (a) and 20000x/ 15000x (b, c, d).	151
Figure 4.16	Sensitivity of mesoporous SnO ₂ (K6-60), SnO ₂ (S15-80) and SnO ₂ (S16-28)-based sensors to 1000 ppm ethanol vapour as a function of operating temperature.	153
Figure 4.17	Small-angle XRD patterns (A) and the corresponding wide-angle XRD patterns (B) of mesoporous SnO ₂ materials replicated from KIT-6 silica template of different hydrothermal aging temperatures; (a) SnO ₂ (K6-80) and (b) SnO ₂ (K6-100).	158
Figure 4.18	N ₂ adsorption-desorption isotherms and the respective pore size distributions (insets) of mesoporous SnO ₂ materials replicated from KIT-6 silica template of different	160

	hydrothermal aging temperatures; (a) SnO ₂ (K6-80) and (b) SnO ₂ (K6-100).	
Figure 4.19	SEM and TEM images of mesoporous SnO ₂ synthesized from KIT-6 silica template at different hydrothermal aging temperatures; (a) SnO ₂ (K6-80) and (b) SnO ₂ (K6-100). Magnification SEM: 20000x/ 15000x, Magnification TEM: 35000x.	161
Figure 4.20	Sensitivity of mesoporous SnO ₂ sensors synthesized from KIT-6 silica template of different hydrothermal aging temperatures as a function of operating temperature.	163
Figure 4.21	TG/DTG-DSC analysis curves of (a) bulk SnCl ₂ •2H ₂ O and (b) KIT-6 silica template infiltrated with an ethanolic SnCl ₂ •2H ₂ O solution in air.	166
Figure 4.22	Small-angle XRD patterns (A) and the corresponding wide-angle XRD patterns (B) of ordered mesoporous SnO ₂ replicas; (a) S(K80)-SLM, (b) S(K80)-CEM and (c) S(K80)-VASEM.	170
Figure 4.23	N ₂ adsorption-desorption isotherms and the respective pore size distributions (insets) of ordered mesoporous SnO ₂ replicas; (a) S(K80)-SLM, (b) S(K80)-CEM and (c) S(K80)-VASEM.	171
Figure 4.24	TEM and SEM images of mesoporous SnO ₂ replicas with different infiltration methods; (a) S(K80)-SLM, (b) S(K80)-CEM and (c) S(K80)-VASEM.	172
Figure 4.25	Sensitivity of mesoporous SnO ₂ (K80)-SLM, SnO ₂ (K80)-CEM and SnO ₂ (K80)-VASEM -based sensors to 1000 ppm ethanol vapour as a function of operating temperature.	173
Figure 4.26	Small-angle XRD patterns of (a) OMS KIT-6-80 template, (b) SnO ₂ (K80)-VASEM(2) replica and (c) 5.0La-SnO ₂ (K80)-V(2)-DS replica.	175
Figure 4.27	Wide-angle XRD patterns of (a) SnO ₂ (K80)-VASEM(2) replica and (b) 5.0La-SnO ₂ (K80)-V(2)-DS replica.	177
Figure 4.28	(A) N ₂ adsorption-desorption isotherms and (B) the corresponding pore size distributions (PSDs) of ordered	179

mesoporous: (a) SnO₂(K80)-VASEM(2) replica and (b) 5.0La-SnO₂(K80)-V(2)-DS replica. Inset Figure 4.28A and 4.8B correspond to KIT-6-80 silica template and their PSDs, respectively.

Figure 4.29	SEM (a and b) and TEM (c and d) images of ordered mesoporous SnO ₂ (K80)-VASEM(2) replica and (b) 5.0La-SnO ₂ (K80)-V(2)-DS replica.	182
Figure 4.30	Sensitivity of 5.0LS(K80)-V(2)-DS sensor towards 500 ppm and 1000 ppm of pure target vapours at different operating temperatures.	184
Figure 4.31	Sensitivity of S(K80)-VASEM(2), 5.0LS(K80)-V(2)-DS and 10.0LS(K80)-V(2)-DS sensors toward various concentrations of pure ethanol and acetone vapour at operating temperature of 300 °C.	190
Figure 4.32	Sensitivity of S(K80)-VASEM(2) and 5.0LS(K80)-V(2)-DS sensors to different ethanol concentrations ranging from 50 ppm to 2000 ppm operated at 300 °C.	192
Figure 4.33	Linear dependence of sensitivity on ethanol vapour concentration for 5.0LS(K80)-V(2)-DS sensor operated at 300 °C.	193
Figure 4.34	Dynamic response of 5.0LS(K80)-V(2)-DS sensor towards 500 ppm ethanol vapour.	195
Figure 4.35	Long-term stability of 5.0LS(K80)-V(2)-DS sensor towards 200 ppm and 500 ppm ethanol vapour at operating temperature of 300 °C.	197

LIST OF ABBREVIATIONS

a.u.	Arbitrary unit
APTS	γ -aminopropyl-triethoxysilane
APTMS	3-aminopropyl-trimethoxysilane
$[\text{AlO}_4]^{5-}$	Aluminate
BET	Brunauer–Emmett–Teller
BJH	Barrett-Joyner-Halenda
CEM	Conventional Evaporation Method
CTAB	Cetyltrimethylammonium Bromide
CTMA	Cetyltrimethylammonium
CVD	Chemical Vapour Deposition
CVI	Chemical Vapour Infiltration
DMF	Dimethylformamide
DRIFTS	Diffuse Reflectance Infrared Fourier Transform Spectroscopy
DS	Direct synthesis
EDX	Energy Dispersive X-ray
EISA	Evaporation-induced self-assembly
EO	Ethylene Oxide
FET	Field-Effect Transistor
F127	Pluronic® 127
GC	Gas Chromatography
GC-MS	Gas chromatography-mass spectrometry
GO	Graphene Oxide
HF	Hydrofluoric Acid
HMS	Hexagonal Mesoporous Silica
HPLC	High-performance liquid chromatography
IM	Impregnation
IUPAC	The International Union of Pure and Applied Chemists
JCPDS	Joint Committee on Powder Diffraction Standards
KIT-n	Korean Institute of Technology

KIT-6	Korean Institute of Technology 6
LC	Liquid-crystal
MCM-41	Mobil Composition Matter no.41
MFC	Mass Flow Controller
MMO	Mesoporous Metal Oxide
MS	Mass spectrometry
MWD	Microwave Digestion
NAFION	Sulfonated Tetrafluoroethylene based Fluoropolymer-Copolymer Membrane
NaOH	Sodium Hydroxide
NASICON	Sodium Super Ionic Conductor
O ₃	Ozone
OMC	Ordered Mesoporous Carbon
OMMOs	Ordered Mesoporous Metal Oxides
OMS	Ordered Mesoporous Silica
OOT	Optimum operating temperature
OSNM	One-step Nanocasting Method
PB-PEO	Polybutadiene-block-poly(ethylene oxide)
PEG	Poly(ethylene glycol)
PEG-PPG-PEG	Poly(ethylene glycol)-block-poly(propylene glycol)-block-poly(ethylene glycol)
PEO	Poly(ethylene oxide)
PF	Phenol-formaldehyde polymers
PIB-b-PEO	Poly(isobutylene) –block- poly(ethylene oxide)
PM	Particulate Matter
PMPEG-PBA	Poly(methoxy poly[ethylene glycol] methacrylate)-block-poly(butyl acrylate)
PPO	Poly(propylene oxide)
PSD	Pore Size Distribution
PTA	Peroxytitanic Acid
PVP	Polyvinyl Pyrrolidone
P123	Pluronic® 123 @ PEG-PPG-PEG
SAXRD	Small-angle X-Ray Diffraction

SBA-n	Santa Barbara Amorphous
SBA-15	Santa Barbara Amorphous 15
SBA-16	Santa Barbara Amorphous 16
SDAs	Structure-directing agents
SDS	Sodium Dodecyl Sulfate
SEM	Scanning Electron Microscopy (SEM)
SnO ₂ (K6-60)	SnO ₂ replicated from KIT-6 silica synthesized at aging temperature of 60 °C
SnO ₂ (S15-80)	SnO ₂ replicated from SBA-15 silica synthesized at aging temperature of 80 °C
SnO ₂ (S16-28)	SnO ₂ replicated from SBA-16 silica synthesized at aging temperature of 28 °C
SnO ₂ (K6-80)	SnO ₂ replicated from KIT-6 silica synthesized at aging temperature of 80 °C
SnO ₂ (K6-100)	SnO ₂ replicated from KIT-6 silica synthesized at aging temperature of 100 °C
S(K80)-SLM	SnO ₂ replicated from KIT-6-80 silica with solid-liquid method
S(K80)-CEM	SnO ₂ replicated from KIT-6-80 silica with conventional evaporation method
S(K80)-VASEM	SnO ₂ replicated from KIT-6-80 silica with vacuum-assisted solvent evaporation method
S(K80)-VASEM(2)	SnO ₂ replicated from KIT-6-80 silica with 2 cycles of vacuum-assisted solvent evaporation method
S(K80)-VASEM(3)	SnO ₂ replicated from KIT-6-80 silica with 3 cycles of vacuum-assisted solvent evaporation method
3.0WS(K80)-V(2)-IM	3.0 wt.% WO ₃ -loaded SnO ₂ via impregnation method
3.0WS(K80)-V(2)-DS	3.0 wt.% WO ₃ -loaded SnO ₂ via direct synthesis
3.0LS(K80)-V(2)-IM	3.0 wt.% La ₂ O ₃ -loaded SnO ₂ via impregnation method
3.0LS(K80)-V(2)-DS	3.0 wt.% La ₂ O ₃ -loaded SnO ₂ via direct synthesis
2.5LS(K80)-V(2)-DS	2.5 wt.% La ₂ O ₃ -loaded SnO ₂ via direct synthesis

5.0LS(K80)-V(2)-DS	5.0 wt.% La ₂ O ₃ -loaded SnO ₂ via direct synthesis
7.5LS(K80)-V(2)-DS	7.5 wt.% La ₂ O ₃ -loaded SnO ₂ via direct synthesis
10.0LS(K80)-V(2)-DS	10.0 wt.% La ₂ O ₃ -loaded SnO ₂ via direct synthesis
SLM	Solid-liquid Method
SMM	Surface Modification Method
SMS	Spherical Mesoporous Silica
SPE	Solid Polymer Electrolyte
[SiO ₄] ⁴⁻	Orthosilicate ion or silicon tetroxide anion
Si(OR) ₄	Tetraalkoxysilane
TEM	Transmission Electron Microscopy
TEOS	Tetraethylorthosilicate
THF	Tetrahydrofuran
Ti(OEt) ₄	Titanium tetraethoxide
TMA	Trimethylamine
TMCS	Trimethylchlorosilane
TSM	Two-solvent Method
TTIP	Titanium isopropoxide
UANM	Ultrasonic-assisted Nanocasting Method
UV-vis DRS	UV-vis diffuse reflectance spectroscopy
VASEM	Vacuum-assisted Solvent Evaporation Method
VOCs	Volatile Organic Compounds
VTS	Vinyltriethoxysilane
WAXRD	Wide-angle X-Ray Diffraction
YSZ	Yttria-stabilized Zirconia
2-D	Two-dimensional
3-D	Three-dimensional

LIST OF SYMBOLS

a_o	XRD unit-cell parameter
d	Pore diameter
d_{100}	d-spacing for (100) reflection
\tilde{d}_{211}	d-spacing for (211) reflection
d_{110}	d-spacing for (110) reflection
D	Average pore size
D	Grain size @ crystallite size
e	Electron
E_g	Band gap
G	Conductance
I	Current
L	Depletion layer thickness
R	Resistance
R_A	Electrical resistance in air
R_{Gas}	Electrical resistance in detected gas
S	Gas sensitivity
S_{etho}	Sensitivity of the sensor to ethanol vapour
S_{ig}	Sensitivity of the sensor to a certain interfering gas or vapour
S_{BET}	BET specific surface area
V	Voltage
V_T	Total pore volume
W	Average pore-wall thickness

PEMBANGUNAN TEMPA NANO OKSIDA TIMAH SEBAGAI PENDERIA GAS BAGI ETANOL DAN ASETON

ABSTRAK

Pemahaman mengenai perilaku penderiaan kebanyakan sensor gas mudah alih yang terdapat di pasaran masih terhad. Kajian penyelidikan ini bertujuan untuk membangunkan tempa nano oksida timah (SnO_2) mesoliang untuk pengesanan gas etanol dan aseton. Untuk mencapai matlamat ini, bahan-bahan SnO_2 mesoliang tersusun telah disediakan melalui kaedah tempa nano dengan menggunakan pra-sintesis silika mesoliang tersusun (OMS) sebagai templat keras. Kesan-kesan parameter tempa nano terhadap sifat pembentukan, struktur dan tekstur SnO_2 mesoliang tersusun, serta keupayaan untuk mengesan wap etanol dikaji dengan menggunakan kaedah satu-faktor-pada-satu-masa. Kestabilan haba SnO_2 mesoliang tersusun juga disiasat pada suhu kalsinasi yang berbeza. Sensor yang difabrikasi dalam bentuk konfigurasi filem tebal oleh SnO_2 mesoliang tersusun selanjutnya diuji untuk pengesanan wap etanol pada suhu operasi antara $150\text{ }^\circ\text{C}$ dan $400\text{ }^\circ\text{C}$. Prestasi pengesanan sensor yang difabrikasi adalah dimaksimumkan di bawah pelbagai parameter operasi. Telah didapati bahawa semua bahan tempa nano SnO_2 mesoliang dipamerkan dengan jelas, mesostruktur tersusun, dan luas permukaan spesifik yang besar serta kerangka kristal yang tinggi. Ini menunjukkan kejayaan proses replikasi daripada templat silika mesoliang tersusun (OMS). Sensor terbaik yang dihasilkan ialah S(K80)-VASEM(2) dengan sensitiviti maksimum sebanyak ~ 28.15 terhadap 1000 ppm etanol pada suhu operasi $300\text{ }^\circ\text{C}$. Sensitiviti sensor S(K80)-VASEM(2) dipertingkatkan lagi dengan memuat 5.0 % berat oksida bes (La_2O_3) ke dalam SnO_2 melalui kaedah sintesis

langsung yang memberikan kepekaan tertinggi sebanyak ~ 52.57. Oksida bes dapat membantu pembentukan rangkaian mesoliat yang tersusun dan stabil, kerangka kristal yang tinggi, kawasan permukaan yang besar dan kehadiran tapak bes. Faktor-faktor ini meningkatkan interaksi antara molekul etanol dan tapak aktif permukaan sensor SnO₂. Ia juga meningkatkan pemilihan dalam tindak balas pengoksidaan etanol yang meningkatkan proses penyah-hidrogenasi. Sensor 5.0LS(K80)-V(2)-DS menunjukkan masa tindak balas yang sederhana iaitu 52 s dan masa pemulihan yang pendek iaitu 43 s serta selektif terhadap wap etanol berbanding aseton. Sensor ini juga menunjukkan kestabilan yang tinggi, keboleholangan dan sensitiviti yang boleh dipercayai selepas penggunaan berterusan selama 14 hari. Semua keputusan menunjukkan bahawa kaedah tempa nano adalah cara yang berkesan dan mudah untuk menyediakan bahan SnO₂ mesoliat tersusun dengan sifat-sifat struktural dan tekstur yang unik dan lebih baik. Sensor yang dihasilkan juga memaparkan prestasi pengesanan gas yang sangat baik dalam mengesan wap etanol.

DEVELOPMENT OF NANOCASTED TIN OXIDE FOR ETHANOL AND ACETONE GAS SENSOR

ABSTRACT

The understanding of sensing behaviour of most portable gas sensors available in the market is still limited. This research study aimed at the development of nanocasted mesoporous tin oxide (SnO_2) for ethanol and acetone gas sensors. To achieve this goal, ordered mesoporous SnO_2 materials were prepared by means of a nanocasting method using pre-synthesized ordered mesoporous silica (OMS) as hard templates. Effects of nanocasting parameters on the formation, structural and textural properties of ordered mesoporous SnO_2 , as well the ability to detect ethanol vapour were studied by employing the one-factor-at-a-time method. The thermal stability of ordered mesoporous SnO_2 was also investigated for different calcination temperatures. The fabricated sensors in the form of thick-film configuration of ordered mesoporous SnO_2 were further tested for ethanol vapour detection at operating temperatures between 150 °C and 400 °C. The sensing performance of the fabricated sensors was maximized under various operating parameters. It was found that all nanocasted mesoporous SnO_2 materials exhibited well-defined, ordered mesostructured, and large specific surface area as well as high crystalline frameworks, indicating successful replication from the OMS templates. The best sensor produced was S(K80)-VASEM(2) with maximum sensitivity of ~28.15 towards 1000 ppm ethanol at an operating temperature of 300 °C. The sensitivity of S(K80)-VASEM(2) sensor was further enhanced by loading 5.0 weight% of basic oxide (La_2O_3) into SnO_2 through direct synthesis that gave the highest sensitivity of ~52.57. The basic oxide could help

the formation of ordered and stable mesoporous networks, high crystalline frameworks, large surface areas and the presence of basic sites. These factors increased the interaction between the ethanol molecules and the surface active sites of the SnO₂ sensor. It also increased the selectivity in ethanol oxidation reaction that increased the dehydrogenation process. The 5.0LS(K80)-V(2)-DS sensor exhibited a moderate response time of 52 s and a short recovery time of 43 s as well as good selectivity to ethanol over acetone vapour. This sensor also demonstrated high stability, repeatability and reliable sensitivity after continuous use for 14 days. All the results showed that the nanocasting method is an effective and a simple way to prepare ordered mesoporous SnO₂ materials with unique and enhanced structural and textural properties. The produced sensors also displayed excellent gas sensing performances in detecting ethanol vapour.

CHAPTER ONE

INTRODUCTION

1.1 Importance of Air Pollutant Monitoring

The increase in pollution and the deteriorating state of our natural atmospheric environment are two consequences of the rapid growth in human population and the increase of industrialisation. There are different types of natural and artificial chemical species in the atmospheric air we live in. In this context, some specified chemical could be harmful to human lives, while the others are vital for our livelihood. For instance, Figure 1.1 outlines the concentration levels of typical gaseous components concerned in Japan (Yamazoe, 2005). The level of humidity and important gases like oxygen (O₂) should be within the sufficient level, however, there is a need to control dangerous gases such as CO, H₂S, CH₃SH, alcohol, VOCs, SO₂, NO₂, CO₂, O₃ so that they are under the designated levels.

Meanwhile, fuel is generated by lower hydrocarbons and H₂, and explosions could occur when these elements are leaked into the air. The main function for gas sensors is to detect the presence of these elements in the air. In this regard, the specified level of concern is 1/10 of lower explosion limit (LEL) for each gas. The standard for air pollutants including volatile organic compounds (VOCs), toxic gases and offensive odours are overseen by different enforcement agents and these standards are determined by the toxicity or hazard level of these gasses, as indicated by star marking in the Figure 1.1. The full line depicts the concentration range that can be safely detected by commercial gas sensor shown and the broken line shows the range that can only be detected in a laboratory test. Over the past two decades, sensory detection has mainly focused on detecting the presence of these dilute components in the air. Some

standards of VOCs such as benzene are seen to be marked under 0.1 ppm, far distant by the present gas sensors.

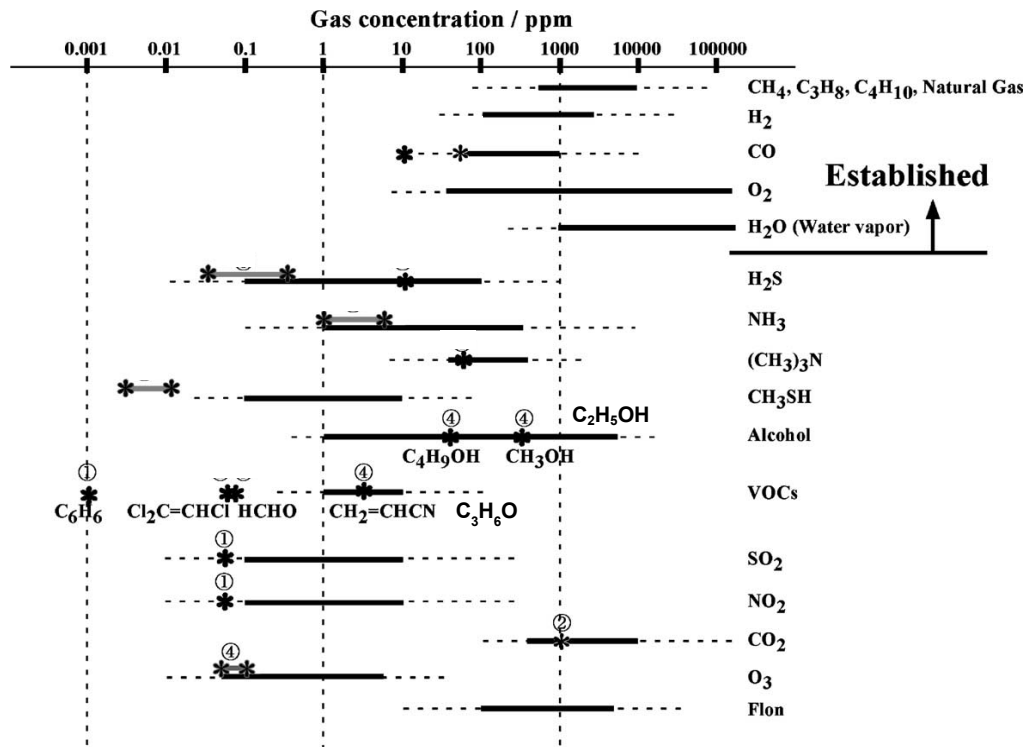


Figure 1.1: Concentration levels of typical gas components concerned in Japan (Yamazoe, 2005).

The global development of industrial and chemical activities can cause radical changes to our everyday lives. Human activities like open burning (e.g. forest fires), the use in pesticides for agricultural activities, emission of fossil fuels, and activities in the petrochemical industry, release toxic and poisonous substances that can bring catastrophic effects to the environment and the human health. These could affect humans in a variety of ways depending on the type and strength of the substance, as well as one's exposure duration to the substance (Hester and Harrison, 1995; DeCaprio, 1999; Katsouyanni, 2003; Cohen *et al.*, 2005; Abadin *et al.*, 2007; Kampa and Castanas, 2008).

Acid rain is one of the harmful environmental effects of air pollutants (Likens and Bormann, 1974; Wu *et al.*, 2006). Acid rain occurs when rain water in a form of precipitation has excessive sulphuric or nitric acids content. Acid rain has dangerous consequences, such as contamination of drinking water, damages to vegetation, destruction of the marine ecosystem, and the corrosion of buildings and structures. Other effects caused by air pollutants are the stratospheric ozone depletion which is accompanying global warming and risks of UV radiation (Dobson, 2005; Mohanakumar, 2008), the greenhouse effect which can also cause global warming (Karl and Trenberth, 2003; Snyder *et al.*, 2009), the ground level ozone (tropospheric ozone) or photochemical smog (Nack and Green, 1974; Amann and Lutz, 2000) and the odour problem (Chapman, 2004).

In our everyday lives, we are increasingly susceptible to breathing, absorbing, and ingesting polluted air, and as a result, toxic and hazardous substances from them could penetrate into our body (Philp, 2013). Hazardous substances tend to remain inside our body, affecting the functions of our lungs, digestive system and skin. Likewise, these substances will either be exhaled or absorbed into our blood to be transported through the various compartments in our body. According to Leghrib (2010), the presence of toxic gases could alter the chemical reactions of individual cells. As a result, one can get the different health problems such as asthma, bronchitis, cancer, kidney and liver damage, skin rashes, cough, throat irritation, birth defects, and miscarriages as shown in Figure 1.2.

For instance, inhaling toxic VOCs, such as benzene, toluene and alcohol fumes originating from burning fossil fuels, particularly from vehicles can elevate one's risk in contracting diseases such as leukaemia and lymphoma (Irigaray *et al.*, 2007), which

are linked to excessive VOCs exposure. In this regard, long-standing contact to VOCs can harm the liver, kidneys and the central nervous system, while short-standing contact to VOCs can cause eye and respiratory tract disturbance, cerebral pain, dazedness, visual confusion, weariness, loss of coordination, unfavorably susceptible skin responses, nausea, and memory hindrance (Guo *et al.*, 2004).

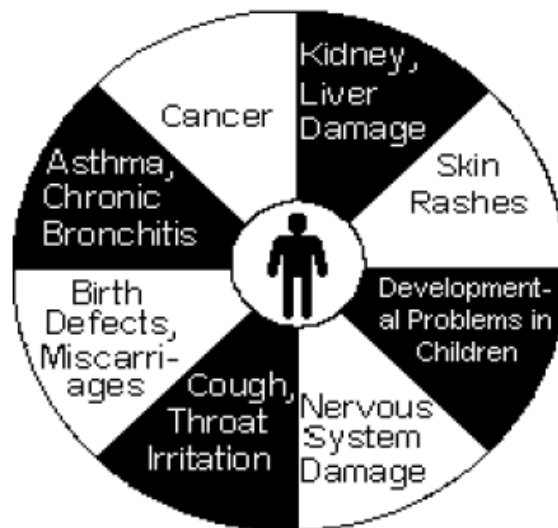


Figure 1.2: Toxic gases effects on human health (Leghrib, 2010).

Nitrogen oxides (NO and NO₂) or commonly symbolised as NO_x are the most well-known and hazardous gaseous contaminants in the atmosphere. One of its traits is that it hard from it to decompose at room temperature. The presence of NO_x can create acid rain that could lead to serious problems including the thinning of the ozone layer. Moreover, NO_x can cause lung irritation and weaken the body's defence against respiratory infections such as pneumonia and influenza (Chauhan *et al.*, 1997; Mauzerall *et al.*, 2005). Carbon monoxide (CO) is mainly produced by incomplete combustion of carbonaceous fuels such as gasoline and natural gas and it can be emitted from vehicles. As one inhales the CO gas, the transport of oxygen to different parts of the body including heart, brain and other important organs is disrupted

(Badman and Jaffé, 1996; WHO, 2000). Then again, exposures to particulate matter (PM) and ozone (O₃) at high fixations are connected to noteworthy death toll anticipation and additionally intense and incessant respiratory and cardiovascular impacts, impeded lung advancement in youngsters, and lessened birth weight (Riediker *et al.*, 2004; Tager *et al.*, 2005).

With the adverse effects on human health as mention above, it can be concluded that air pollutants contribute to increased mortality and hospital admissions. In this regard, after the first United Nations (UN) Conference on the Environment in Stockholm which was held in June 1972 (Declaration, 1972), the general public has progressively developed an understanding over the importance of preserving the environment. The 1990s saw the rapid change of attitudes within the industry as the public began to realise the importance of preserving the environment, health, and workers' safety and sparked a global call for decrease the toxic gases exposure limit to limit the health treats they cause. This justifies the need to find the most effective way for measuring air contaminants levels in both outdoor and indoor environment. Hence, the detection and monitoring system is critically needed to identify and control the emission of air pollutants.

1.2 Detection and Monitoring System

A great attention for executing detecting devices in order to enhance environmental and safety control of gases in domestic and industrial applications has been concerned nowadays. In this regard, there are two sorts of identification system usually utilized for observing and monitoring poisonous gases, which are traditional analytical instrument and solid-state gas sensors.

1.2.1 Conventional Analytical Instrument

Today, some established analytical methods are being utilized capably to screen and monitor the environment contaminant level. For example, gas phase chromatograph (GC) (Raghuram *et al.*, 2010), gas chromatography-mass spectrometry (GC-MS) (Araújo *et al.*, 2010), mass spectrometry (MS) (Taylor and Linforth, 2003) and Fourier transforms infrared (FTIR) instruments (Bak and Clausen, 2002).

All these instruments give genuinely exact and particular gas readings. Nonetheless, they require skilled and knowledgeable operators, are mostly extremely costly, and intended for laboratory tabletops or specific on-line applications for in-plant installations. Additionally, these instruments include complex and dreary procedures and are timewasting despite the fact that they have many advantages. A large number of them suffer from limitations, for example, high cost, high maintenance, slow response time and vast size to make them unpractical monitors in area of air quality and security (Lee and Lee, 2001; Li *et al.*, 2010).

A basic, quick and high-sensitivity on-line monitoring device for the toxic gases is required. Without a doubt, a portable sensor such as solid-state gas sensor is a standout amongst the most viable strategies and electronic devices for gas real-time monitoring. Meanwhile, solid-state gas sensors can be combined with other forms of detection system to detect the presence of toxic gasses and control their emission. These sensors use a sensing layer which interacts with gas and detects the presence of gas, subsequently, this chemical interaction will be turned into electrical signals (Leghrib, 2010). The following section discusses about the available types of solid-state gas sensor and a new trend of mesoporous metal oxides as sensing material for detecting toxic gases.

1.2.2 Solid-State Gas Sensors

Solid-state gas sensors are favourable in the development of commercial gas sensors where they are widely applied in automotive, process control, medical diagnosis, environmental sensing, household applications, personal safety and national security (Moseley, 1997; Gaskov and Rumyantseva, 2000; Capone *et al.*, 2003; Moos *et al.*, 2009; Ho, 2011). They are one of the vital technologies in modern life. The sensing materials that are utilized in these sensors will change their properties depending on the ambient gas. One of the first solid-state gas sensors was introduced in 1962, where thin-film ZnO and porous SnO₂ ceramics were used as part of the gas-sensing devices. Over the last 40 years, this device has gone through numerous developmental phases (Seiyama and Kato, 1962). In this regard, solid-state gas sensors are compact, robust, and adaptable and are inexpensive. These features make them ideal as micro-arrays to detect various different gas compositions in the environment (Hu *et al.*, 2010).

In view of the sensing principles and materials, solid-state gas sensors can be categorized into the accompanying three principle classes: (i) solid-electrolyte gas sensors, (ii) capacitor-type gas sensors and (iii) semiconductor gas sensors. The first class is solid-electrolyte gas sensors, where the species to be detected affects the Nernst potential or changes the ionic current flowing through solids (Nernst, 1899). In this regard, the conductivity of solid electrolytes is stemmed from mobile ions rather than electrons and is typically dominated by only one type of ion. In general, solid electrolytes allow the quantitative determination of the concentration of chemical species that are ionically transferred in the electrolyte (Lin, 1997).

The second class is capacitor-type gas sensors. A capacitor-type gas sensor is a form of field-effect device that can measure the changes in the dielectric film constant between the electrodes as a function of gas concentrations. The changes of the capacitance in this typically sensors are normally within the pF range and depend on the operating frequency and surrounding conditions including the level of humidity and temperature (Lee and Lee, 2001). Currently, the most widely used of capacitor-type gas sensors are metal-oxide-semiconductor (MOS) capacitors and transistors (MOSFETs) (Hu *et al.*, 2010).

The third class and the most widely studied area of solid-state gas sensors is semiconductor gas sensors. These sensors are based on semiconducting metal oxides. In this regard, the reaction caused by the adsorption of a gaseous species by a semiconducting surface will create surface states which change the electrical properties (Morrison, 1982). Over the years, there are several significant progresses in using the change in the semiconductor properties as a way to measure the existence of a particular reactive gas in a gaseous mixture. Contrasted with the organic semiconductors (β -naphthol, phenanthrene, polyimide, polyamide, polyimidazole, polybenzimidole and so on) and elemental or compound semiconductors (Si, Ge, GaP, GaAs, and so on.), the semiconducting metal oxide colleagues have been more effectively exploited as sensing materials for the detection and measuring of numerous gases such as CO, CO₂, H₂, H₂O, NH₃, SO_x, NO_x and alcohols (Azad *et al.*, 1992). The sensing material is usually deposited as a polycrystalline film or layer on a substrate with integrated electrodes and heating. The working principle of these sensors is accepted to be founded on the possibility that, other than by the reaction with oxygen, the surface and grain boundary resistance of the oxide is controlled by the adsorption of the gaseous species (Seiyama and Kato, 1962). Moreover, the

chemical adsorption is very discriminating for various reactive gases. The adequacy of these sensors relies upon a few factors including the idea of the reaction occurring at the oxide surface, the catalytic properties of the surface, the electronic properties of the bulk oxide, the temperature, and the microstructure (Moseley, 1997).

Table 1.1 summarizes the applications of solid-state gas sensors and the choice of sensing materials for each type of gas sensor. From the table, it can be concluded that among the solid-state gas sensors, semiconductor gas sensors have been widely used for all gases detected. Special attention is paid to the semiconductor gas sensors type over the others owing to its advantages of low fabrication cost, small size, simple structure, ease of integration, good stability and low energy consumption (Capone *et al.*, 2003; Shi *et al.*, 2009a).

1.3 Metal Oxide-based Semiconductor Gas Sensors

Metal oxides embody a different and engaging class of materials which properties cover the whole range from metals to semiconductors and insulators and nearly all parts of material science and physics in ranges including superconductivity and magnetism (Comini, 2006). In the field of chemical sensing, metal oxides are frequently exploited as functional sensing materials for semiconductor gas sensors due to fact that the electrical conductivity or resistivity of metal oxides varies with the composition of the gas atmosphere surrounding them. These materials and its reaction with gases are first introduced by Brattain and Bardeen (1953), and Heiland (1957) in 1950's (Brattain and Bardeen, 1953; Heiland, 1957). Later, Bielanski and co-worker (1957), and Seiyama and Kato (1962) introduced the direct applications of metal oxide as catalyst and electric conductive detectors towards various gases (Bielanski *et al.*, 1957; Seiyama and Kato, 1962) and brought to the market by Taguchi (Taguchi, 1972).

Table 1.1: Solid-state gas sensors for detecting environmental gases (Hu *et al.*, 2010).

Detected Gas	Types of Sensors	Sensing Materials	References
SO ₂	Semiconductor type	CeO ₂ , SnO ₂ , Ag doped-WO ₃ , NiO-SnO ₂ .	(Várhegyi <i>et al.</i> , 1995), (Berger <i>et al.</i> , 1997), (Shimizu <i>et al.</i> , 2001), (Hidalgo <i>et al.</i> , 2005)
	Solid-electrolyte type	Na-β-alumina, Ag-β"-alumina, NASICON-ZnSnO ₃ , Ag ⁺ ion-Ag ₂ SO ₄ .	(Akila and Jacob, 1989), (Yang <i>et al.</i> , 1996), (Zhong <i>et al.</i> , 2008), (Uneme <i>et al.</i> , 2011).
H ₂ S	Semiconductor type	CuO/SnO ₂ , CdO-doped ZnO/TiO ₂ , Pd/La-doped In ₂ O ₃ .	(Liu <i>et al.</i> , 2003), (Bodade <i>et al.</i> , 2008), (Kapse <i>et al.</i> , 2009).
	Solid-electrolyte type	SPE-Pt, NAFION-H ₂ SO ₄ , NASICON/Pr ₆ O ₁₁ -SnO ₂ .	(Yourong <i>et al.</i> , 2001), (Yu <i>et al.</i> , 2002), (Liang <i>et al.</i> , 2007).
CO ₂	Semiconductor type	La ₂ O ₃ -coated SnO ₂ , Pd/Al ₂ O ₃ -doped TiO ₂ , CaO-loaded In ₂ O ₃ , Ag-added BaTiO ₃ -CuO.	(Kim <i>et al.</i> , 2000), (Chaudhari <i>et al.</i> , 2006), (Prim <i>et al.</i> , 2007), (Herrán <i>et al.</i> , 2008).
	Solid-electrolyte type	NASICON/Na ₂ CO ₃ -BaCO ₃ , NASICON/Li ₂ CO ₃ -BaCO ₃ , NASICON/BiCuVO _x -CaTiO ₃	(Wang and Kumar, 2003), (He <i>et al.</i> , 2007), (Kishi <i>et al.</i> , 2007).
	Capacitor type	NiO/PbO/Y ₂ O ₃ /CuO-BaTiO ₃ , CeO-BaCO ₃ /CuO.	(Ishihara <i>et al.</i> , 1995a; Wei <i>et al.</i> , 2000), (Matsubara <i>et al.</i> , 2000).
CO	Semiconductor type	La ₂ O ₃ /CuO-anatase TiO ₂ , CeO ₂ -ZnO, V-SnO ₂ , Co ₃ O ₄ .	(Savage <i>et al.</i> , 2001), (Al-Kuhaili <i>et al.</i> , 2008), (Wang and Chen, 2010), (Vetter <i>et al.</i> , 2015).
NO ₂	Semiconductor type	Au/Ti-doped In ₂ O ₃ , Cr-doped TiO ₂ , WO ₃ -SnO ₂ , ZnO-SnO ₂ .	(Steffes <i>et al.</i> , 2001), (Ruiz <i>et al.</i> , 2003), (Bai <i>et al.</i> , 2010), (Hwang <i>et al.</i> , 2010).
	Solid-electrolyte type	Y ₂ O ₃ -ZrO ₂ /LaFeO ₃ , Y ₂ O ₃ -ZrO ₂ /ZnFe ₂ O ₄ or ZnCr ₂ O ₄ , Y ₂ O ₃ -ZrO ₂ /NiO, NASICON/Au/ITO/NaNO ₂ - Li ₂ CO ₃ .	(Yoon <i>et al.</i> , 2001), (Zhuiykov <i>et al.</i> , 2002), (Miura <i>et al.</i> , 2006), (Obata and Matsushima, 2008).
	Capacitor type	NiO/ZnO, NaNO ₂ -Ca ₃ (PO ₄) ₂ -WO ₃ .	(Ishihara <i>et al.</i> , 1995b), (Zamani <i>et al.</i> , 2005).

Table 1.1: (Continued)

Detected Gas	Types of Sensors	Sensing Materials	References
NO	Semiconductor type	Bi ₂ O ₃ -doped WO ₃ , Ag-doped WO ₃ , In ₂ O ₃ -SnO ₂ , In ₂ O ₃ -ZnO.	(Tomchenko <i>et al.</i> , 1998), (Chen and Tsang, 2003), (McCue and Ying, 2007), (Lin <i>et al.</i> , 2010).
	Solid-electrolyte type	Y ₂ O ₃ -ZrO ₂ /CdCr ₂ O ₄ , NASICON/ SmFeO ₃ -Au, Ni/Co-doped LaGaO ₃ .	(Lu <i>et al.</i> , 1997), (Kotzeva and Kumar, 2003), (Dutta and Ishihara, 2005).
	Capacitor type	Pd-added SrSnO ₃ -WO ₃ .	(Ishihara <i>et al.</i> , 2000)
O ₃	Semiconductor type	WO ₃ , Zn ₂ In ₂ O ₅ -MgIn ₂ O ₄ , SmFeO ₃ , SnO ₂ , ZnO.	(Cantalini <i>et al.</i> , 2000), (Miyata <i>et al.</i> , 2000), (Hosoya <i>et al.</i> , 2005), (Korotcenkov <i>et al.</i> , 2007a), (Catto <i>et al.</i> , 2015).
	Capacitor type	Phthalocyanine-based FET	(Bouvet <i>et al.</i> , 2001).
Alcohols/ VOCs	Semiconductor type	ZnO, TiO ₂ , Sr-added NiAl ₂ O ₄ , Fe-doped SnO ₂ , La/Er/Yb-doped In ₂ O ₃ .	(Wan <i>et al.</i> , 2004), (Rella <i>et al.</i> , 2007), (Vijaya <i>et al.</i> , 2008), (Wang and Liu, 2009), (Zhang <i>et al.</i> , 2013).
	Solid-electrolyte type	Sulfonic acid-GO, NASICON/ZnTiO ₃ , BiCuVO _x /perovskite oxide.	(Jiang <i>et al.</i> , 2016), (Zhong <i>et al.</i> , 2014), (Kida <i>et al.</i> , 2009).

The basic detection principles of metal oxide-based semiconductor gas sensors are illustrated in Figure 1.3. The sensors reversibly change their conductivity (or resistance) because of changes in gas concentration and subsequently give data about the composition of the surrounding atmosphere. They work at between 100 and 500 °C and have been basically utilized as a part of genuine conditions (at atmospheric pressure and at a high background oxygen concentration of 20.5 vol%). The sensor activity is communicated as sensor response (changes in resistance, R) and called sensitivity (S). For n-type semiconductor oxides, the sensitivity is expressed as $S = R_{Gas}/R_A$ or $S = R_A/R_{Gas}$ for oxidizing and reducing gases, respectively, while it is the other way around for the p-type semiconductor oxides.

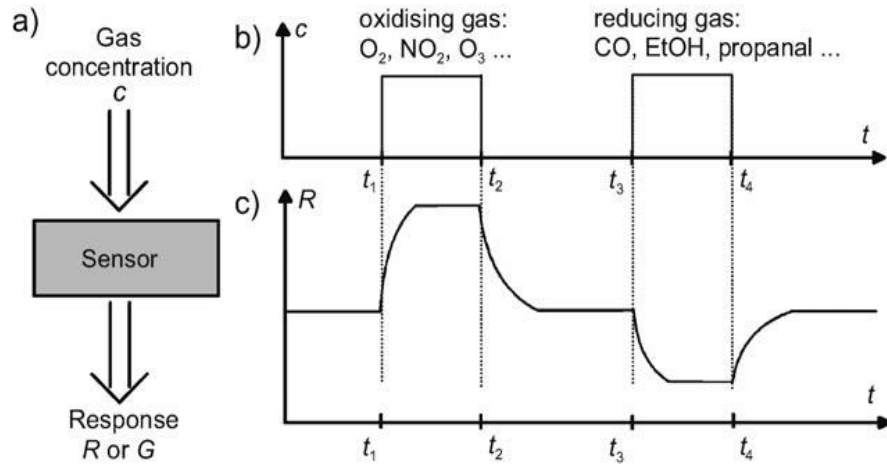


Figure 1.3: (a) the changes in the gas concentration of metal oxide-based semiconductor gas sensor with n-type conductivity; (b) the gas is applied at t_1 , t_3 and removed at t_2 , t_4 ; (c) lead to changes in the conductance G or resistance R of the sensor (Gurlo and Riedel, 2007).

It is believed that change in conductivity or resistivity of the sensor when exposed to gas atmosphere is due to change in charge carrier concentration of the sensing materials (metal oxides) and it depends on the type of conductivity of the metal oxides. The metal oxides can have either n-type or p-type semiconductor of conductivity. An n-type semiconductor is a material that dominant part of charge carriers are electrons, and upon contact with a reducing gas, an increase in conductivity or a decrease in resistance take place. A p-type semiconductor is a material that conducts with positive holes being the larger part charge carriers. Thus, the inverse impacts are seen in this material and demonstrating an expansion in conductivity or a decline in resistance with the existence of an oxidizing gas where the gas has expanded the quantity of positive holes. An increment of resistance with a reducing gas is detected, where the negative charge brought into the material decreases the concentration of positive hole charge carrier. A summary of the resistance response towards gas atmosphere is given in Table 1.2.

Table 1.2: Sign of resistance change (increase or decrease) to change in gas atmosphere (Williams, 1999).

Metal oxides	Oxidizing gases	Reducing gases
n-type	Resistance 	Resistance 
p-type	Resistance 	Resistance 

Table 1.3 summarizes the classification of metal oxides based on the type of conductivity. From the table, it is noted that those SnO₂, ZnO, In₂O₃, WO₃ and TiO₂ are commonly used for the fabrication of gas sensor materials are classified into the n-type semiconductor conductivity. In general, n-type oxides are thermally stable and have the capability to work at lower oxygen partial pressure as compared to p-type oxides (Korotcenkov, 2007). It is known that p-type oxides are relatively unstable because of the tendency to exchange lattice oxygen easily with air (Madou and Morrison, 2012). But, it does not mean that the p-type oxides are not applicable for sensor design. Few works has shown that p-type oxides are excellent materials in detecting H₂S and CH₄ (Pratt and Williams, 1997; Ivanovskaya *et al.*, 2003; Chen *et al.*, 2008).

Table 1.3: Classification of metal oxides based on type of conductivity (Korotcenkov, 2007).

Type of conductivity	Metal oxides
n-type	MgO, CaO, TiO ₂ , ZrO ₂ , V ₂ O ₅ , Nb ₂ O ₅ , Ta ₂ O ₅ , MoO ₃ , WO ₃ , ZnO, Al ₂ O ₃ , Ga ₂ O ₃ , In ₂ O ₃ , SnO ₂
p-type	Y ₂ O ₃ , La ₂ O ₃ , CeO ₂ , Mn ₂ O ₃ , Co ₃ O ₄ , NiO, PdO, Ag ₂ O, Bi ₂ O ₃ , Sb ₂ O ₃ , TeO ₂
n, p-type	HfO ₂ , Cr ₂ O ₃ , Fe ₂ O ₃ , CuO

Metal oxides exhibit various electro-physical features, ranging from insulators to wide band-gap semiconductors (Kanan *et al.*, 2009). These features are the vital factors that make the metal oxide suitable to be used as a gas sensor. The big band gap

(E_g) and small activation energy of the centers is the optimal combination of parameters for the materials designed for metal oxide-based semiconductor gas sensors. This is necessary to avoid the sensor's operation in the region of self-conductance. As reported by Korotcenkov (2007), the optimal band gap for the metal oxide must be greater than 2.5 eV to operate at temperatures exceeding 300 °C. Table 1.4 shows the band gaps of various metal oxides used as sensing materials. Hence, it can be concluded that those well-known metal oxides satisfy the requirement for a gas sensor criterion. Besides, it is necessary to note that the band gap for n-type oxides may act as a donor band while p-type oxides act as an acceptor band (Trimboli, 2005).

Table 1.4: Band gap of metal oxide used as sensing materials (Korotcenkov, 2007).

Metal oxides semiconductor	Band gap (eV)
MgO, CaO, Al ₂ O ₃ , SiO ₂ , TeO ₂	> 6.0
SrO, Y ₂ O ₃ , HfO ₂ , ZrO ₂	5 – 6
BaO, La ₂ O ₃ , CeO ₂ , Ga ₂ O ₃	4 – 5
TiO ₂ , Nb ₂ O ₅ , Ta ₂ O ₅ , ZnO, In ₂ O ₃ , SnO ₂	3 – 4
V ₂ O ₅ , Cr ₂ O ₃ , WO ₃ , NiO, Fe ₂ O ₃	2 – 3
Co ₃ O ₄ , PdO, CuO, Sb ₂ O ₃	1 – 2

Nowadays, there are a lot work that have been done to study the gas-sensing performance of metal oxides towards detection of various hazardous gases including CO, H₂S, NO, NO₂, SO₂, CO₂, O₃ and VOCs. Figure 1.4 demonstrates the relative examination of references, accessible in the open literature, on the gas-sensing properties of all the metal oxides considered. The tin oxide (SnO₂) is the most widely investigated material with 35% of the research endeavors. The following significant oxide material that has drawn more consideration is the mixed oxides at 13%. Zinc oxides (ZnO) are at 10%, trailed by titanium oxides (TiO₂) and tungsten oxides (WO₃) at 7% each, indium oxides (In₂O₃) at 5%, iron oxides (Fe₂O₃), gallium oxides (Ga₂O₃),

and niobium oxides (NbO_2) are at 3% each. Oxides of zirconium (ZrO_2), molybdenum (MoO_2), copper (CuO), cerium (CeO_2), and aluminum (Al_2O_3) are at 2%. Further oxides such as bismuth, cadmium, cobalt, chromium, and nickel oxides (Bi_2O_3 , CdO , Co_3O_4 , Cr_2O_3 , and NiO) are at 4%.

Every material has its advantages and they should be wisely selected according to their utility in gas sensor applications. However, in this research work, SnO_2 had been chosen as the metal oxide to be used as sensing material owing to its low cost and high sensitivities for different gas species. SnO_2 is categorized into the n-type semiconductor with the favoured output signal for detection of reducing gases.

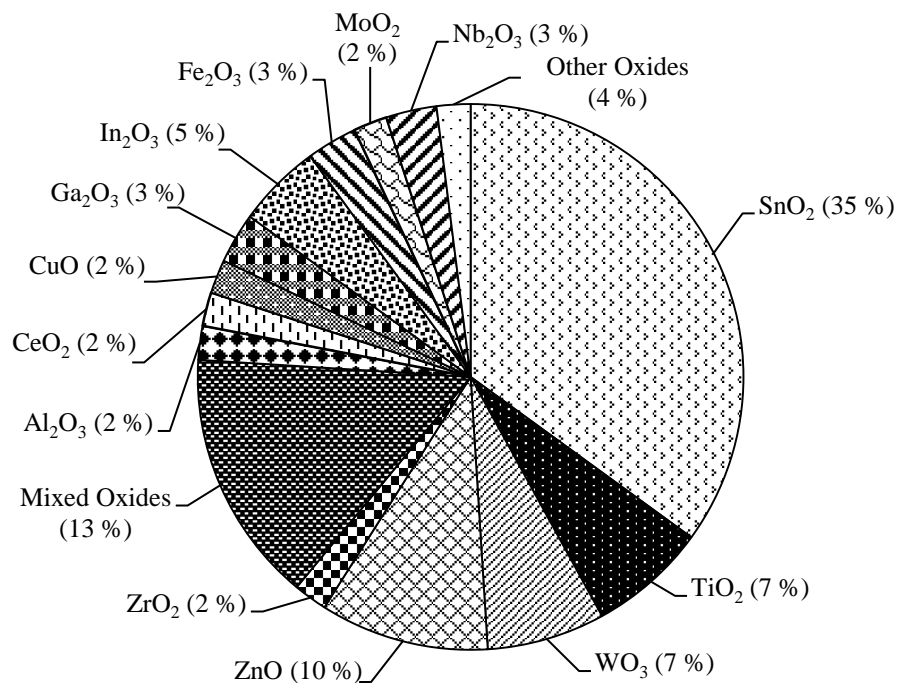


Figure 1.4: Relative comparison of different metal oxides used for gas-sensing application (Eranna *et al.*, 2004).

1.4 Mesoporous Metal Oxides

Since the discovery of ordered mesoporous silica such as MCM-41 and SBA-15 in the 1990s (Beck *et al.*, 1992; Zhao *et al.*, 1998a), interests in the preparation of non-siliceous mesoporous materials have been tremendously expanded (Lu *et al.*, 2005; Jiao *et al.*, 2008; Rushton and Mokaya, 2008; Doi *et al.*, 2010; Yang *et al.*, 2010). Metal oxide materials with mesoporous structures that have pore size between in 2–50 nm (Sing, 1998) can be considered as nanomaterials since the pores are in the nanoscale. These oxides are increasingly used in wide range of applications such as in catalysis (Jin *et al.*, 2012b; Rosen *et al.*, 2014), adsorption and separation (Wang and Lo, 2009a; Konishi *et al.*, 2009), gas sensors (Wagner *et al.*, 2009; Li *et al.*, 2014), drug delivery and molecular imaging (Wang *et al.*, 2013b; Tang *et al.*, 2012) as well as storage devices (Zhang *et al.*, 2015). Apart from being used in novel applications and devices, mesoporous oxides are progressively used as alternatives to conventional materials due to their inexpensive, more efficient and easier to produce (Nawrocki *et al.*, 2004a; Nawrocki *et al.*, 2004b; Stratakis and Kymakis, 2013).

A mesoporous metal oxide has a large surface area, a narrow pore size distribution and a high surface-to-volume ratio. As a result, these oxides have a high surface energy, high grain boundaries and excellent optical properties. This shows their promising use in the industry, for instance, the large surface area and the semi-conducting feature of mesoporous TiO₂ can be combined and used in a dye-sensitized solar cells to harvest energy from sunlight (Jose *et al.*, 2009). The high surface areas and relatively large pores of mesoporous metal oxides which allow a high concentration of active sites per mass of material and facilitate mass transfer are extremely beneficial for catalysing reactions (Taguchi and Schuth, 2005). This large

surface area enables catalytic agents to be highly dispersed on the surface, which is highly desirable in the catalysis community.

Mesoporous metal oxides have a high surface to volume ratio due to their large surface area and narrow sized pores. This increases the diffusion rate, making them ideal for separation and adsorption process. Moreover, their large surface area and high porosity make them useful for the delivery of drugs where they are used as a medium for releasing drug compounds to diseased cells (Vallet-Regí, 2006). However, some mesoporous polymers would deform at temperature exceeding 400 °C and this would affect their performance while mesoporous silica will experience sintering at extremely high temperatures (about 600 °C). In this regard, mesoporous metal oxide materials have higher durability and thermal stability and are able to maintain their integrity and mechanical strength at such high temperatures (Lee *et al.*, 2008). The thermal stability allows processes to be carried out at high temperatures, and this is critical for gas sensing applications since the gas sensors are usually operated at elevated temperatures of up to 500 °C. Meanwhile, the durable nature of porous metal oxides creates a stable platform that has a wide pH range, making it suitable for different uses such as for chromatography (Barteau, 1996).

1.5 Problem Statement

Gas sensors have been used in different fields such as to detect ethanol vapour in wine production and in breath analysers that are used to detect drunk drivers. At present, many researchers are focusing on developing low-cost, small size, highly sensitive and accurate portable ethanol gas sensors (Zhan *et al.*, 2007; Tang *et al.*, 2007). This is because conventional gas detecting systems such as optical spectroscopy and gas chromatography/spectroscopy (Phillips and Greenberg, 1987; Lopez *et al.*,

2002) are either time-consuming, require large size and expensive analytical systems. In this light, gas sensors with unique structure such as with high mesoporosity could have improved their performances (Jiao *et al.*, 2008; Waitz *et al.*, 2010). Over the past few years, researchers have been introducing gas sensors with mesoporous metal oxides (MMOs) to overcome the drawbacks associated with conventional sensors. It was claimed that MMOs have ordered structures, tunable pore sizes, high thermal stabilities and crystalline frameworks that could offer large surface areas and better interconnectivity. Hence, it is believed that the use MMOs as sensing materials in this study could possibly improve the sensor performances in detecting ethanol vapour.

In the meantime, there are many portable ethanol gas sensors available in the market. These sensors often use n-type metal oxides such as SnO₂, In₂O₃, ZnO, TiO₂ and Fe₂O₃ as sensing materials. Most portable sensors could be fabricated cheaply, easy to operate and have high stability. However, these sensors usually demonstrated moderate sensitivity, low response, slow recovery time and high operating temperature. To overcome these drawbacks, this study attempted an alternative way to produce MMOs with excellent structural and textural properties by a nanocasting method. Based on previous works, performances of metal oxides-based semiconductor gas sensors could be intensely influenced by surface properties and structural features (Korotcenkov, 2005; Korotcenkov, 2008). Past works have shown that porous structure increased the amount of active surface area and competent gas diffusion which could enhance gas-sensing performance (Tiemann, 2007; Wagner *et al.*, 2013a).

At present, MMOs for gas-sensing applications are synthesized through conventional sol-gel synthesis routes (Vuong *et al.*, 2004), chemical vapour deposition (CVD) (Liu *et al.*, 2005), spray pyrolysis (Tani *et al.*, 2002; Korotcenkov *et al.*, 2007a)

and precipitation reactions (Pinna *et al.*, 2004) that resulted in MMOs with low surface area, poor thermal stability and an ill-defined mesostructure. On the other hand, Shimizu *et al.* (2005) and Hung *et al.* (2010) used soft-templating method by using the surfactants or block co-polymers as structure-directing agents to produce MMOs with enhanced structural properties. However, it was claimed that this process was not able to prepare numerous MMOs because the metal precursors were easier to be hydrolysed, had poor condensation, weak redox reactions, weak connection with the surfactants, phase transitions and the thermal breakdown of the structural integrity. The resulting MMOs had poor mesostructure regularity and were thermally unstable. Moreover, the MMOs produced had amorphous or semi-crystalline walls that could limit their application in gas sensors.

Typically, a precursor solution for the targeted metal oxide is infiltrated into the mesopores of the hard templates. After drying the solvent, the composite is usually heated at a certain temperature in order to convert the precursor into oxide and the hard template will be finally removed by using chemical treatment using hydrofluoric acid (HF) or sodium hydroxide (NaOH), yielding MMOs as its negative replica. This process is called nanocasting in which the pre-synthesized ordered mesoporous silica (OMS) or ordered mesoporous carbon (OMC) materials are utilized as the hard templates. Meanwhile, OMCs are more commonly used as the hard templates due to the fact that carbon can effectively be expelled during calcinations and the metal oxide structure will remain (Schüth, 2003). The hydrophobic property of carbon also makes it troublesome for OMC materials to be totally loaded with the metal precursor. Hence, there is a need to determine whether OMC or OMS materials are suitable as hard templates for the nanocasting process. Furthermore, the nanocasting process reported in previous works used various infiltration techniques including solid-liquid method

(SLM) (Yue and Zhou, 2007), one-step nanocasting method (OSNM) (Yang *et al.*, 2003a), conventional evaporation method (CEM) (Dickinson *et al.*, 2006), two-solvent method (TSM) (Imperor-Clerc *et al.*, 2004), surface modification method (SMM) (Zhu *et al.*, 2003), ultrasonic irradiation (Deng *et al.*, 2010) and supercritical fluid solution-phase (Crowley *et al.*, 2003) method. It has been reported that these methods could still be unable to achieve complete filling of the silica mesopore with the metal precursors and some have limitations in practical applications due to the difficulty of the experimental process.

Based on the above argument, this study is one of the first studies that will develop ethanol gas sensors that use nanocasted mesoporous SnO₂ for fast and accurate selective detection of ethanol vapour. As the existing sensors still have significant limitations, it is believed that it will be meaningful to study the ethanol-sensing performances of ordered mesoporous SnO₂ prepared by the nanocasting method. Through this method, OMS materials with channel-type mesopores from SBA-n and KIT-n families are used as hard templates due to their open pore structure that could allow the precursors to be filled equally into the channel-type pores.

In this study, attempts were also made to improve the infiltration technique by using the vacuum-assisted solvent evaporation method (VASEM) that could improve the capillary force during the nanocasting process. It was believed that this infiltration technique would produce superior ordering of nanocasted mesoporous SnO₂ compared to the previously reported mesoporous SnO₂ (Cabot *et al.*, 2004; Satishkumar *et al.*, 2009; Shon *et al.*, 2009b). Moreover, to improve the ethanol-sensing performances of ordered mesoporous SnO₂, a basic oxide i.e. lanthanum oxide (La₂O₃) that could address the reaction towards the dehydrogenation route was included in the sensor

design. Until recently, the use of ordered mesoporous La-loaded SnO₂ nanocasted from OMS KIT-6 as sensing material for detection of ethanol vapour has never been addressed.

1.6 Research Objectives

The current research work has been planned to meet the following objectives:

- a) To synthesize and characterize nanocasted mesoporous SnO₂ materials using pre-synthesized ordered mesoporous silica (OMS) as a hard template.
- b) To study the effect of different nanocasting parameters on the formation of nanocasted mesoporous SnO₂ materials including their structural and textural properties as well as the sensor's sensitivity towards ethanol vapour.
- c) To determine maximum gas-sensing performances of nanocasted mesoporous SnO₂ materials under various operating parameters.
- d) To elucidate gas-sensing mechanism of the optimum sensor of nanocasted mesoporous SnO₂ materials.

1.7 Scope of the Study

The present study is conducted in three main research components consist of the preparation, characterization and gas-sensing performance of ordered mesoporous sensing materials. Each of research study is wisely scheduled and implemented to fulfil the outlined research objectives. Preparation of sensing materials involves the syntheses of ordered mesoporous silica (OMS) that subsequently to be used as a hard template for nanocasting of ordered mesoporous metal oxide of SnO₂. In the present study, the selection of mesoporous SnO₂ as the sensing material is based on its high sensitivity due to their large surface-to-volume ratio, high chemical stability under

harsh conditions, low cost in fabrication and successful application as sensor material by other researchers. The nanocasting method is chosen to produce mesoporous SnO₂ materials with large surface areas, ordered pore systems and well-defined structures. This method uses a hard template from OMS to obtain the desired pattern of structures of the SnO₂.

Effects of type of OMS, hydrothermal aging temperature of OMS, infiltration method, cycle of infiltration step, additive loading technique and additive loading on the formation of ordered mesoporous SnO₂ including their structural and textural properties as well as ethanol-sensing performances are investigated thoroughly. By using one-factor-at-a-time method, the optimized sensing materials with ability to get well-ordered structure and good response to ethanol vapour have been obtained. Thermal stability of the optimized sensing materials by calcination at different temperatures is also studied. Comprehensive characterizations of the sensing materials including powder X-ray diffraction (P-XRD), N₂ adsorption/desorption, transmission electron microscopy (TEM) and scanning electron microscopy (SEM) are essential at this part in order to confirm the presence of ordered structure within the sensing materials and eventually to evaluate the quality of the produced ordered mesoporous SnO₂ via nanocasting method. Auxiliary sensor material characterizations inclusive of thermogravimetric analysis (TGA), differential scanning calorimetric (DSC) and UV-vis diffuse reflectance spectroscopy (UV-vis DRS) are also investigated to provide the supplementary information on the structural and textural properties of sensing materials that can be correlated to the overall sensor performances and gas-sensing mechanism.

The produced ordered mesoporous SnO₂ are used to form thick films prior to be tested for gas sensors. A series of continuous gas-sensing measurements are conducted to investigate the sensing performance of ordered mesoporous SnO₂ sensor against air pollutants detection. The sensor measurement is done in a gas chamber provided with heating facilities, connected to an electrometer and upgraded data logging system. Ethanol and acetone vapours are selected as model air pollutants to be detected. The concentration of vapours is analysed using a gas chromatograph before the vapours are injecting into the gas chamber for the sensor measurement. The parameters studied at this stage are optimum operating temperature, selectivity towards different vapours, variation of vapour concentrations, response and recovery times and last but not least the stability or reliability of the thick film sensors. The sensor performance is evaluated based on the electrical resistance and the sensitivity have been calculated under different conditions. A gas-sensing mechanism for optimum sensor has been proposed.

1.8 Organization of the Thesis

This thesis is put together in five major chapters. Each chapter represents an integral part of the main work that is sequentially arranged. In order to assist the reader, this thesis is organized as follows:

Chapter 1 gives an outline of the whole thesis which includes the importance of air pollutant monitoring, the detection and monitoring system that are used and available in worldwide, an introduction to metal oxide based semiconductor gas sensors and a utilization of mesoporous metal oxides as sensor materials in the current gas sensors technology. This chapter also enclose with problem statement to illustrate the rationale and significant of the research and to identify the clear direction of

research objectives. The scope of study and organization of the thesis provides the general idea for the whole research.

Chapter 2 presents the comprehensive review on the interconnected research works. The first part of the chapter elaborated in details the progress of porous materials particularly towards an ordered mesoporous metal oxides in modern history, synthesis method and applications. The concept of soft-templating and hard-templating (nanocasting) method in creation of ordered mesostructured metal oxides are well elaborated. Details synthesis via nanocasting method using ordered mesoporous silica as hard template and the parameters involved are described. In a meanwhile, the second part summarizes the role of mesoporous structure in gas sensing application followed by specificity of ordered mesoporous SnO₂ as sensor materials and its sensing mechanism. Finally, the structural and gas sensing properties of ordered mesoporous SnO₂ as well as the effect of surface doping on SnO₂ also discussed.

Chapter 3 describes the experimental methodology and analysis. The details of materials, chemicals, gases and equipment used throughout the research work are given. This chapter is divided into several parts to represent sensor material syntheses and preparation, thick film fabrication, sensor material characterizations, sensor performance measurements and procedures as well as operating parameter studied.

Chapter 4 is the core body of the thesis that discusses, interprets and analyses the results obtained in the present studies. This chapter embraces of several parts, which are covers the findings on the synthesis and characterization of silica templates, nanocasting of ordered mesoporous SnO₂ with different silica templates, infiltration